# P2.62 A SIMULATION OF PARTIAL CLOUDINESS IN MULTILAYERED ALTOCUMULI

Michael J. Falk, Vincent E. Larson
University of Wisconsin–Milwaukee *

## Abstract

This paper seeks to gain understanding of what processes influence the cloud fraction of altocumulus clouds. Our starting point is a cloud system observed on 25 June 1996 during the CLEX-1 field experiment. This two-layered system comprised a partly cloudy cumuliform layer located about 500 meters below an overcast stratiform layer. This cloud system was documented with aircraft data and simulated in three dimensions with high resolution using the COAMPS-LES model. Given observed initial atmospheric profiles, the model successfully simulates the qualitative structure of the layered system, although the modeled cumuliform layer has less cloud fraction, liquid water, and turbulence than the observations.

Next, sensitivity studies were performed using the COAMPS-LES model. These gave evidence that partial cloudiness in our simulations is caused primarily by conditional instability and the consequent vertical motions of air parcels within the layer.

This mechanism is complicated by the presence of radiative heating and cooling. When the lower cloud layer is heated radiatively throughout its entire depth, it becomes conditionally unstable and partly cloudy. This is true even if the layer is initially overcast and absolutely stable, and even if the radiative heating rates are small. However, the *entire* lower layer heats only if there is an upper cloud layer above. If the upper layer is removed, then the lower layer cloud top cools strongly to space, and the lower layer remains overcast. Through this radiative effect, the presence or absence of an upper layer influences the cloud fraction of a lower layer, even though the two layers are spatially separated and have little dynamical interaction.

## 1. INTRODUCTION

Understanding partly cloudy altocumulus clouds is of interest for several reasons. One is that the subject of altocumuli is fertile ground for basic scientific inquiry. Altocumuli have been studied far less than stratocumulus or cirrus clouds (Larson et al. 2006), but nevertheless are a common cloud type, covering 22% of the sky worldwide (Warren et al. 1988a,b)., but they have been studied far less than stratocumulus or cirrus clouds (Larson et al. 2006). Studying altocumuli also has practical motivations; for instance, altocumuli hamper operations of unmanned aerial vehicles (UAVs) in at least two ways (Fleishauer et al. 2002). First, supercooled altocumuli can cause icing on aircraft wings, which particularly endangers UAVs that are small. Second, when high-altitude UAVs are used for reconnaissance, altocumuli can obstruct the ground from view. The degree of obstruction depends on cloud fraction. In principle, UAV missions can be planned on the basis of forecasts, but a recent study (Zhang and Co-Authors 2005) showed that large-scale models greatly underpredict the occurrence of altocumuli.

The present paper's focus is on how altocumuli develop partial cloudiness. For a partly cloudy layer to exist, there must exist horizontal variability in either temperature or moisture, so that some regions are saturated and some are not. One possible mechanism of formation is that a layer which contains pre-existing variability in relative humidity is cooled and becomes saturated in the moister regions. Although this mechanism may be important, we do not discuss it in the present paper. Rather, we focus on internal mechanisms of generating variability in moisture. In particular, we explore how conditional instability affects partial cloudiness and how radiative heating, in turn, affects conditional instability.

An outline of the rest of this paper is as follows. Section 2 provides an overview of the case and the aircraft observations. Section 3 discusses our simulations of the observed cloud. Section 4 uses sensitivity experiments to explore the effects of conditional instability and radiation on cloud fraction. Section 5 lists conclusions and implications for cloud parameterization in large-scale models.

## 2. CASE BACKGROUND AND AIRCRAFT DATA

The first Complex Layered Cloud Experiment (CLEX-1) provided in-situ observations of non-precipitating mid-level clouds. On 25 June 1996, CLEX-1 sampled a two-layer altocumulus cloud system over eastern Kansas that provides the basis of the present paper.

The size and structure of the cloud system were as follows. At 1631 UTC, the horizontal extent of the system was about 900 $km^2$ (Figure 1). The two layers were distinct, separated by several hundred meters. The lower cloud layer was partly cloudy and cumuliform, with cloud base at approximately 5500 m above sea level (ASL) and cloud thicknesses of 200 to 300 m. The upper cloud layer was completely overcast and stratiform,

* *Corresponding author address:* Michael J. Falk, Atmospheric Science Group, Department of Mathematical Sciences, University of Wisconsin — Milwaukee, P. O. Box 413, Milwaukee, WI 53201-0413, USA; email: mjfalk@uwm.edu

with cloud base at approximately 6000 m ASL and cloud thickness of 300 to 500 m (Figure 2). We define overcast as the condition where there are no lines of sight from ground to sky that are unobscured by cloud. The elements of the upper layer appeared to have rounded tops, and turbulence formed within the cloud. The cloud system was first measured by the aircraft at about 1630 UTC, but the system was already dissipating by this time. By 1800 UTC, the lower layer had dissipated entirely and the upper layer had diminished in size (Tulich 1998).

In-situ measurements of the cloud system and its vicinity were obtained by the University of Wyoming King Air (UWKA) aircraft. Measurements of temperature, moisture, pressure, wind, and particle concentration were taken every second from 1607 to 1812 UTC on 25 June 1996; the aircraft was actually in the cloud system from approximately 1630 to 1800 UTC. In processing the aircraft data, we used the pressure data from the altimeter, the temperature data from a Minco reverse-flow sensor, dew point data as computed from the Cambridge chilled-mirror hygrometer, cloud droplet data as computed from the forward-scattering spectrometer probe (FSSP), and ice crystal data from Particle Measuring Systems' 2D-C and 2D-P optical array probes.

We regarded the most reliable measurements to be time averages over straight, level flight legs. We considered legs to be straight if their heading varied by no more than $20^\circ$, and level if their altitude above sea level varied by no more than 10 m. We were able to isolate seven level flight legs (Figure 3), some with two or three components (straight and located at the same height but separated by an aircraft turn). We also filled in a data gap by using one level flight leg which was not straight. From these legs, we reconstructed a sounding representing the cloud system. Additionally, some data from above the highest flight leg was obtained from a slow, spiral descent the aircraft made through the cloud system.

An important forcing mechanism for mid-level clouds is large-scale ascent or subsidence (Larson et al. 2001). However, measuring vertical velocity averaged over the cloud system with our aircraft data was not feasible. Therefore, to estimate large-scale vertical motion, we used reanalysis data (Figure 4). To provide some measure of uncertainty, we used data from three reanalyses: the National Centers for Environmental Prediction/National Center for Atmospheric Research (NCEP/NCAR) Reanalysis, the National Centers for Environmental Prediction/Department of Energy (NCEP/DOE) Reanalysis-II, and European Centre for Medium-range Weather Forecast (ECMWF) ERA-40 Re-analysis. These were obtained from National Center for Atmospheric Research. In order to interpolate these gridded analyses to the location of the cloud system, we used the Barnes scheme (Barnes 1964). The reanalyses show that the cloud system was located in a region of ascent during its formation early in the day on 25 June 1996, but by the time the aircraft began sampling the system, there was descent. These data were used to force the large-scale vertical motion in our simulations.

Because our clouds were colder than freezing, one might ask whether ice processes were important. To address this, we computed the concentration of ice crystals of different sizes and separated them into bins by diameter. The total amount of ice present was much smaller than the amount of liquid water; on most legs, the ice water mixing ratio was about 1000 times smaller than the liquid water mixing ratio. In the leg with the most ice (leg 4, in the upper cloud layer), the ice water mixing ratio was 0.002 g $kg^{-1}$ and the ice number concentration was 0.87 $L^{-1}$. For this leg, we plotted the number concentration of ice particles in each bin in Figure 5. This figure illustrates that the larger ice particles had diameters of up to hundreds of microns. To estimate the importance of ice in the cloud, we performed a simple back-of-the-envelope calculation of the time required for ice diffusional growth to deplete all liquid. The time calculated was 8 hours for the iciest leg but 51 hours for the least icy leg. Thus, for simplicity in this initial study, our simulations assumed that our clouds consisted entirely of supercooled water droplets and neglected the effects of ice.

## 3. A SIMULATION OF THE OBSERVED CASE

### *3.1 The COAMPS-LES model*

Numerical simulations of the 25 June 1996 were conducted using the Coupled Ocean/Atmosphere Mesoscale Prediction System (COAMPS$^{\mathrm{TM}}$) Large-Eddy Simulation (COAMPS-LES) model. COAMPS-LES is a modification of the COAMPS mesoscale model to include subgrid-scale mixing, enabling the model to accurately simulate fields on fine grid scales (Golaz et al. 2005). It has performed comparably to other LES models in simulations of boundary layer clouds such as the Atlantic Trade Wind Experiment (ATEX) (Stevens and Co-Authors 2001), Barbados Oceanographic and Meteorological Experiment (BOMEX) (Siebesma and Co-authors 2003), Atmospheric Radiation Measurement Project (ARM) (Brown and Co-authors 2002), First ISLSCP (International Satellite Land-Surface Climatology Project) Regional Experiment (FIRE) (Moeng et al. 1996), and Dynamics and Chemistry of Marine Stratocumulus Phase II (DYCOMS-II) (Stevens and Co-authors 2003).

A second-order advection scheme was used for momentum variables while a positive definite scheme was used for scalar variables. We applied the anelastic approximation, a generalization to vertically stratified atmospheres of the Boussinesq approximation. The anelastic approximation removes sound waves.

Our simulations were run on an 81x81 horizontal grid, with gridpoints separated by 50 m. There were 201 vertical gridpoints, separated by 12.5 m. We used a one-second timestep.

### 3.2 Radiative heating scheme

The longwave radiative transfer scheme that we have implemented in COAMPS-LES is an analytic formula (Larson et al. 2006) that is a modification of Stevens and Co-Authors (2005). Our shortwave radiative flux scheme was that used in the EUROCS stratocumulus intercomparison (Duynkerke and Co-Authors 2004), originally based on Shettle and Weinman (1970).

To verify that our analytical radiation scheme was realistic, we compared it to BUGSrad, a sophisticated, two-stream, numerical radiative transfer code (Stephens et al. 2001, 2004). We fed each scheme the profile of clouds and thermodynamics averaged over the first hour after spinup and then compared both schemes. total heating rate (longwave + shortwave) profiles (Figure 6).

Qualitatively, BUGSrad and the analytical radiation scheme agree well. In the upper cloud layer, both schemes produce cooling of about 3 K hr$^{-1}$ near the top and weaker warming of 1 to 2 K hr$^{-1}$ near the base. The cloud-top cooling arises because cloud-top parcels emit significant amounts of longwave radiation to space, for which they receive no radiation in return. The loss of energy leads to cooling. In the lower cloud layer, both schemes predict weak warming and no cooling throughout the entire cloud depth. The fact that there is no cooling in the lower layer is important for basic features of its structure, as we will see in Section 4 below. The weak warming results because the lower layer receives substantial longwave radiation from the ground below, which is much warmer than the cloud. There is no cooling near the cloud-top of the lower layer, but radiation emitted upward is nearly counterbalanced by downwelling radiation from the upper layer.

### 3.3 Initial conditions and spinup

We used the aircraft data to construct the sounding used for model initialization. The temperature, height, moisture, and wind were averaged over each straight, level flight leg, and then the averages were arranged vertically to construct a profile. Although the aircraft measurements were not exactly spatially and temporally collocated, they all occurred within about 50 km and one hour of one another (see Figure 3). Therefore, we treated them as if they were collocated horizontally and temporally. The model was initialized in an idealized fashion in which all fields were horizontally uniform, except for temperature, which was randomly perturbed to initiate the turbulence. Therefore, at the initial time, each grid layer was either overcast or clear. The model was allowed to spin up for an hour, during which there was an initial burst of turbulence and subsequent equilibration. After the model spinup, the mean fields of the model were compared with the observations from the aircraft legs to ensure that they matched well.

Figure 7 shows comparisons between the observed (diamonds) and the simulated (dashed line) total water mixing ratio ($r_t$), potential temperature ($\theta$), and liquid water potential temperature ($\theta_l$). Additionally, for observations which were computed from averages of flight legs, the crosses on the chart mark the range within which 68% of the observed data points lie, and the circles mark the range within which 95% of the observed data points lie. These annotations show clearly how much variance was present in the observed data.

The simulation matches the observed data well at many altitudes but there are some minor discrepancies. Wherever the observed data had sharp gradients (for instance, where a very dry layer of air was located between two moister layers), the simulation tends to "smooth" the profile by bringing the high and low values closer together. Other than this smoothing, the simulated and observed data agree well. This agreement is expected, since $r_t$, $\theta$, and $\theta_l$ were prescribed in the model at the initial time.

### 3.4 Model simulation of cloud layers

Next, we test the model's ability to simulate liquid-water mixing ratio ($r_l$), in-cloud liquid-water mixing ratio ($r_l$ / $C$), cloud fraction ($C$), and standard deviation of vertical velocity $w$, $\sqrt{\overline{w'^2}}$. (High values of ($\sqrt{\overline{w'^2}}$) indicate high levels of turbulence.) To do so, we compare observations at the initial time with simulated profiles in the hour after spinup (Figure 8). The fact that we are comparing a simulated profile that has evolved one to two hours beyond the observed profile is a drawback. However, the comparison is still useful qualitatively.

Within the upper cloud layer, $r_l$, $C$, and $\sqrt{\overline{w'^2}}$ are simulated with qualitative accuracy. As expected, the simulated cloud is located higher because it is rises via ascent and entrainment during the first hours of the simulation. Within the lower cloud layer, $r_l$, $C$, and $\sqrt{\overline{w'^2}}$ are underpredicted. These problems are related: if more clouds form, they will generate more turbulence.

The underprediction of $r_l$ and $C$ is related to the fact that the simulated atmosphere is too homogeneous in the cumuliform layer. The model correctly predicts the total water mixing ratio ($r_t$), but does not properly predict the wide range of values about the mean (not shown). Since the lower layer is subsaturated in the mean, liquid forms only where moisture is anomalously large. The simulation's underprediction of moisture variability implies an underprediction of high-moisture parcels, and consequently an underprediction of $r_l$ and $C$.

The simulated in-cloud liquid-water mixing ratio ($r_l/C$) for the lower cloud layer matches the observations better than does $r_l$ or $C$ alone. This shows that the simulation predicts a reasonable amount of liquid water within cloud, but does not predict enough liquid water and cloud fraction overall.

Why does the simulation have less $r_l$, $C$, and $\sqrt{\overline{w'^2}}$ than the observations? One possible explanation is that the model is unable to produce enough horizontal variability, perhaps because the horizontally homogeneous initialization is unrealistic, or perhaps because

the model's horizontal domain is too small. However, it is quite possible that the observed estimates of $r_l$, $C$, and $\sqrt{\overline{w'^2}}$ are too high, for two reasons. First, the flight tracks may not have randomly sampled the atmosphere, but rather preferentially sampled cloud. Simple averaging of flight legs, as we have done, would then lead to an overestimate of $r_l$, $C$, and $\sqrt{\overline{w'^2}}$. Second, the large-scale ascent that we use to force the simulation may be too small. The reanalyses we use were all calculated on a coarse grid with a grid spacing of 200 to 275 km. Averaging over a large grid box homogenizes the vertical velocity field and diminishes the maxima and minima. This is significant because while turbulence appears to be less sensitive, the large-scale ascent rate strongly increases cloud fraction and liquid water (Figure 9).

Finally, vertical motion data is not explicitly measured; it must be inferred from quasi-geostrophic theory and thus the vertical motion calculations are subject to the assumptions and approximations of quasi-geostrophic theory. In particular, quasi-geostrophic theory does not consider the vertical motions associated with gravity waves.

## 4. THE CAUSES OF PARTIAL CLOUDINESS IN OUR SIMULATIONS: SENSITIVITY EXPERIMENTS

In this section, we investigate how cloud fraction is influenced by atmospheric stability, radiative transfer, and the presence of multiple cloud layers. We suspect that conditional instability plays a role because it promotes vertical motion of air parcels, which in turn enhances the cloudiness of ascending parcels and the dryness of descending parcels. We also suspect that the radiative heating of the lower layer is important because first, radiative heating may lead to conditional instability, and second, the radiation preferentially heats parcels with more liquid, leading to vertical motion of air parcels and possibly partial cloudiness.

### *4.1 Base case*

The simulation of the 25 June 1996 altocumulus cloud system that we have discussed thus far is denoted the "base case". (Figure 10). The temperature profile in this case is absolutely stable in the upper layer, which is stratiform, but conditionally unstable in the lower layer, which is cumuliform. The upper layer remains overcast in all our sensitivity simulations, but the cloud fraction of the lower layer varies widely between simulations.

We treat the base case as a qualitatively reasonable approximation of the actual atmospheric state on 25 June 1996. All of the following experiments are modifications of the base case.

### *4.2 Is partial cloudiness in our simulation caused by conditional instability?*

In the base case, the lower layer was partly cloudy after the spin-up period. Was its partial cloudiness due to conditional instability in the initial profile, a radiative effect, or a combination of both? To isolate the effects of instability, we performed the two following simulations in which all radiative transfer is turned off.

#### 4.2.1 Base case, no radiation

This sensitivity experiment (Figure 11) omits radiative transfer but is otherwise identical to the base case. In particular, there is still conditional instability in the lower cloud layer at the initial time.

The lower cloud is initialized as an overcast, horizontally uniform layer, but it becomes partly cloudy during the spin-up period and maintains low cloud fraction until it dissipates. The fact that partial cloudiness forms while radiative transfer is shut off demonstrates that radiative transfer is not necessary to generate partial cloudiness in this case, and that conditional instability is sufficient.

The lack of radiative transfer in the present case does introduce some comparatively minor differences from the base case. First, the present case has higher cloud fraction in the cumuliform layer early in the simulation. Presumably this is because the lack of radiative heating allows the lower layer to remain cooler than it would otherwise, causing more condensation for direct thermodynamic reasons. The temperature changes little between simulations because condensation releases latent heat. Second, in the present simulation the height of the upper (stratiform) layer stays nearly constant instead of rising. This is because without radiation, there is little generation of turbulence in the upper layer and hence little entrainment. Without entrainment — that is, without the incorporation of clear air above the cloud into the cloud itself — the cloud layer cannot grow upward.

#### 4.2.2 Initially stable case, no radiation

In this sensitivity experiment, radiative transfer is still shut off, but now we make the lower cloud layer absolutely stable at the initial time, as described below. Whereas the prior experiment showed that if instability is present, then an overcast layer can become partly cloudy, here we investigate a related question: If an overcast layer is absolutely stable, then does the layer remain overcast?

To remove the lower-layer instability, we modified the profile so that the temperature lapse rate between the model base and the base of the upper cloud is 5 K km$^{-1}$, which is absolutely stable to moist convection. Since such a drastic cooling of the temperature profile also changes the amount of liquid water, we modified the profile of total water mixing ratio in order to keep the relative humidity and liquid water virtually unchanged.

This initially stable simulation (Figure 12) produces an overcast lower layer, in contrast to what was produced by the conditionally unstable base case with and without radiation (Sections 4.1 and 4.2.1). Therefore, the present simulation illustrates that stability can lead to an overcast cloud layer, whereas the prior sensitivity simulation (Section 4.2.1) illustrated that instability can lead to a partly cloudy layer. Taken collectively, these two simulations indicate a strong relationship between conditional instability and cloud fraction.

In the present case, although the lower layer remains overcast in the sense that there is never a clear-sky line of sight from above cloud to the ground, the upper region of the layer becomes partly cloudy. Initially, without any conditional instability to promote mixing between the clear air and the lower cloud, those two layers stay separated and do not mix to create a partly cloudy region. After a few hours, the uppermost portion of the lower cloud warms enough due to microphysical interactions that it becomes very slightly conditionally unstable, and so the small amount of partial cloudiness between 5700 and 5800 m forms. The region of the cloud which becomes unstable also becomes partially cloudy, but the remainder of the cloud stays completely stable and thus stays completely overcast.

The location of the conditional instability within the cloud affects the formation of cumuliform clouds. When instability occurs at the bottom of a cloudy layer but stability forms at the top of the layer, the stability acts as a cap which prevents buoyant parcels from rising out of the cloud and mixing with the clear region above cloud top, thus inhibiting cumuliform development. But, when instability occurs at the top of the cloudy region, the cloudy and clear air mix and a cumuliform region develops. In this case, the presence of conditional instability is correlated with the development of partly cloudy cumuliform clouds, and the presence of stability is correlated with the maintenance of completely overcast stratiform clouds.

## *4.3 How does the presence of an upper cloud layer affect the cloud fraction of a lower layer?*

The previous sensitivity experiments (Sections 4.2.1 and 4.2.2) isolated the effects of conditional instability by shutting off radiative transfer. However, radiative heating and cooling are important in part because they modify the temperature profile and thus the stability of the atmosphere. In the following two sensitivity experiments we turn on radiative heating and cooling and make the lower layer initially stable. We find that the profile of radiative heating strongly influences the lower cloud dynamics and cloud fraction. This radiative profile, however, depends on the presence or absence of a cloud layer above.

### 4.3.1 Initially stable case, with radiation

This sensitivity experiment is identical to the initially stable case (Section 4.2.2), except that radiation is turned on. In the initially stable case, the lower cloud layer remained overcast. In contrast, when radiation is turned on, as in the present case, the lower layer becomes partly cloudy (Figure 13). In fact, the present case looks similar to the (conditionally unstable) base case, with its partly cloudy, cumuliform lower layer (Figure 10). How does radiative transfer cause partial cloudiness in an initially stable profile?

Radiative transfer causes radiative heating throughout the depth of the lower layer. This radiative heating, though small, modifies the temperature profile over time, causing the initially stable layer to become conditionally unstable. Then the lower cloud layer breaks up into cumuliform cloud.

The upper cloud layer cools at its top and warms at its bottom, creating instability and turbulence within cloud, but it does not develop a cumuliform region because of the strong, stable cloud-top inversion.

### 4.3.2 Initially stable case, with radiation and one layer

This sensitivity experiment is identical to the previous one (4.3.1) except that the upper cloud layer is entirely removed. This was accomplished by decreasing the total water mixing ratio within the upper-level cloud. Previously, with the upper layer present, the lower layer became partly cloudy. Here, with the upper layer removed, the lower layer remains overcast (Figure 14). Why is this?

When both an upper and a lower cloud layer are present, the lower cloud layer undergoes radiative warming throughout its entire depth, creating instability. But when the upper layer is absent, the lower layer's radiative heating profile changes. Instead of warming everywhere, it warms at its base and cools at its top, as does the upper layer in the base case and the initially stable case. Instability is created within cloud but a strong, stable inversion sets up at cloud top. Because of this, the cloud stays overcast and stratiform.

In this case (Figure 14),the cloud layer becomes turbulent, but because of the location of the instability within cloud, moist parcels are less likely to mix with dry air, creating a partially cloudy region.

Simply removing the upper cloud layer changes the cloud morphology of the lower layer drastically, despite the fact that the two layers are only weakly dynamically linked. Their only interaction is through radiative processes. The lower layer's cloud-top warming, present only when the upper layer is present, is the mechanism allowing instability and cumuliform development; in the absence of the upper layer, the lower layer undergoes cloud-top cooling to space, a stable inversion is created immediately above cloud top, and the layer stays completely overcast and stratiform.

## 5. CONCLUSIONS

We have performed large-eddy simulations (LES) of a two-layered altocumulus system that was observed on 25 June 1996. The simulations provide a qualitatively useful representation of the observed cloud layers, although the simulations do predict less horizontal variability, cloud fraction, and liquid water in the lower layer than observed.

Starting from this base case simulation, we performed sensitivity experiments in which radiative transfer was turned on or off, the initial stability of the lower layer was modified, and the upper layer was removed. Our primary finding is that conditional instability promotes partly cloudy cumuliform clouds and that absolutely stability promotes overcast, stratiform clouds.

This finding, however, is complicated by radiative transfer. Even small radiative heating or cooling rates can, over a period of several hours, alter the stability of a layer. The radiative heating or cooling profile, in turn, depends on the presence or absence of other cloud layers. Specifically, when a nearby upper layer is present, the lower layer experiences radiative heating throughout its depth, causing the development of conditional instability. In our simulation, the resulting cloud is cumuliform with a cloud fraction of less than about 40%. When no upper layer is present, the lower layer experiences radiative cooling to space near cloud top. This cooling favors the development of a cloud-top inversion, which in turn inhibits the upward rise of parcels and keeps the layer overcast.

In this way, a dramatic change in cloud fraction and morphology is caused by a purely radiative interaction between upper and lower cloud layers. The two layers are physically separated and have little dynamical interaction.

If it is true that partly cloudy altocumulus layers can be generated by small-scale, internal processes, as opposed to pre-existing variability in relative humidity, then this has implications for parameterization of mid-level layer clouds in large-scale models, i.e. those models with horizontal grid spacing greater than 10 km. Namely, it suggests that parameterizations ought to contain a realistic coupling between subgrid thermodynamics (i.e. moisture and temperature fields) and subgrid dynamics (i.e. turbulence and turbulent fluxes). The subgrid thermodynamics in the parameterization must properly drive the subgrid dynamics because, given the unstable thermodynamic profile, the parameterization must be capable of generating accurate dynamics (turbulent updrafts and downdrafts). That is, the parameterization's thermodynamic profile must properly drive the dynamics. Conversely, the dynamics must accurately drive the thermodynamics. Namely, the turbulent transport must correctly alter the thermodynamic variability and mean profile. While boundary layer parameterizations contain such subgrid interactions, it is unknown whether present-day mid-level "stratiform" cloud parameterizations contain sufficiently accurate coupling.

So, after all, what causes partial cloudiness to form in multilayered altocumuli? Directly, the answer is "conditional instability," but the presence of conditional instability is strongly dependent on radiative heating or cooling profiles, and in particular the radiative interaction between upper and lower cloud layers.

## References


Barnes, S. L., 1964: A technique for maximizing details in numerical weather map analysis. *J. Appl. Meteor.*, **3**, 396–409.

Brown, A. R. and Co-authors, 2002: Large-eddy simulation of the diurnal cycle of shallow cumulus convection overland. *Quart. J. Roy. Meteor. Soc.*, **128**, 1075–1093.

Duynkerke, P. G. and Co-Authors, 2004: Observations and numerical simulations of the diurnal cycle of the EUROCS stratocumulus case. *Quart. J. Roy. Meteor. Soc.*, **130**, 3269–3296.

Fleishauer, R. P., V. E. Larson, and T. H. Vonder Haar, 2002: Observed microphysical structure of midlevel, mixed-phase clouds. *J. Atmos. Sci.*, **59**, 1779–1804.

Golaz, J.-C., S. Wang, J. D. Doyle, and J. M. Schmidt, 2005: Second and third moment vertical velocity budgets derived from COAMPS-LES. *Bound.-Layer Meteor.*, **116**, 487–517.

Larson, V. E., R. P. Fleishauer, J. A. Kankiewicz, D. L. Reinke, and T. H. Vonder Haar, 2001: The death of an altocumulus cloud. *Geophys. Res. Lett.*, **28**, 2609–2612.

Larson, V. E., K. E. Kotenberg, and N. B. Wood, 2006: An analytic longwave radiation formula for liquid layer clouds. Submitted to *Mon. Wea. Rev.*

Moeng, C.-H., W. R. Cotton, A. Chlond, M. Kairoutdinov, S. Krueger, W. S. Lewellen, M. K. MacVean, J. R. M. Pasquier, H. A. Rand, A. P. Siebesma, B. Stevens, and R. I. Sykes, 1996: Simulation of a stratocumulus-topped planetary boundary layer: Intercomparison among different numerical codes. *Bull. Amer. Meteor. Soc.*, **77**, 261–278.

Shettle, E. P. and J. A. Weinman, 1970: The transfer of solar irradiance through inhomogeneous turbid atmospheres evaluated by Eddington's approximation. *J. Atmos. Sci.*, **27**, 1048–1055.

Siebesma, A. P. and Co-authors, 2003: A large eddy simulation intercomparison study of shallow cumulus convection. *J. Atmos. Sci.*, **60**, 1201–1219.

Stephens, G. L., P. M. Gabriel, and P. T. Partain, 2001: Parameterization of atmospheric radiative transfer. Part I: Validity of simple models. *J. Atmos. Sci.*, **58**, 3391–3409.

Stephens, G. L., N. Wood, and P. Gabriel, 2004: An assessment of the parameterization of subgrid-scale cloud effects on radiative transfer. Part I: Vertical overlap. *J. Atmos. Sci.*, **61**, 715–732.

Stevens, B. and Co-Authors, 2001: Simulations of trade wind cumuli under a strong inversion. *J. Atmos. Sci.*, **58**, 1870–1891.

Stevens, B. and Co-authors, 2003: Dynamics and chemistry of marine stratocumulus DYCOMS-II. *Bull. Amer. Meteor. Soc.*, **84**, 579–593.

Stevens, B. and Co-Authors, 2005: Evaluation of large-eddy simulations via observations of nocturnal marine stratocumulus. *Mon. Wea. Rev.*, **133**, 1443–1462.

Tulich, S. N., 1998: Measured and calculated structures of a multi-layer altocumulus cloud. CSU Atmos. Sci. Paper 647, Colorado State University. 190 pp.

Warren, S. G., C. J. Hahn, J. London, R. M. Chervin, and R. Jenne, 1988a: Global distribution of total cloud cover and cloud type amount over land. Technical report, NCAR TN-317 STR.

Warren, S. G., C. J. Hahn, J. London, R. M. Chervin, and R. Jenne, 1988b: Global distribution of total cloud cover and cloud type amount over the ocean. Technical report, NCAR TN-317 STR.

Zhang, M. H. and Co-Authors, 2005: Comparing clouds and their seasonal variations in 10 atmospheric general circulation models with satellite measurements. *J. Geophys. Res.*, **110**, doi:10.1029/2004JD005021.

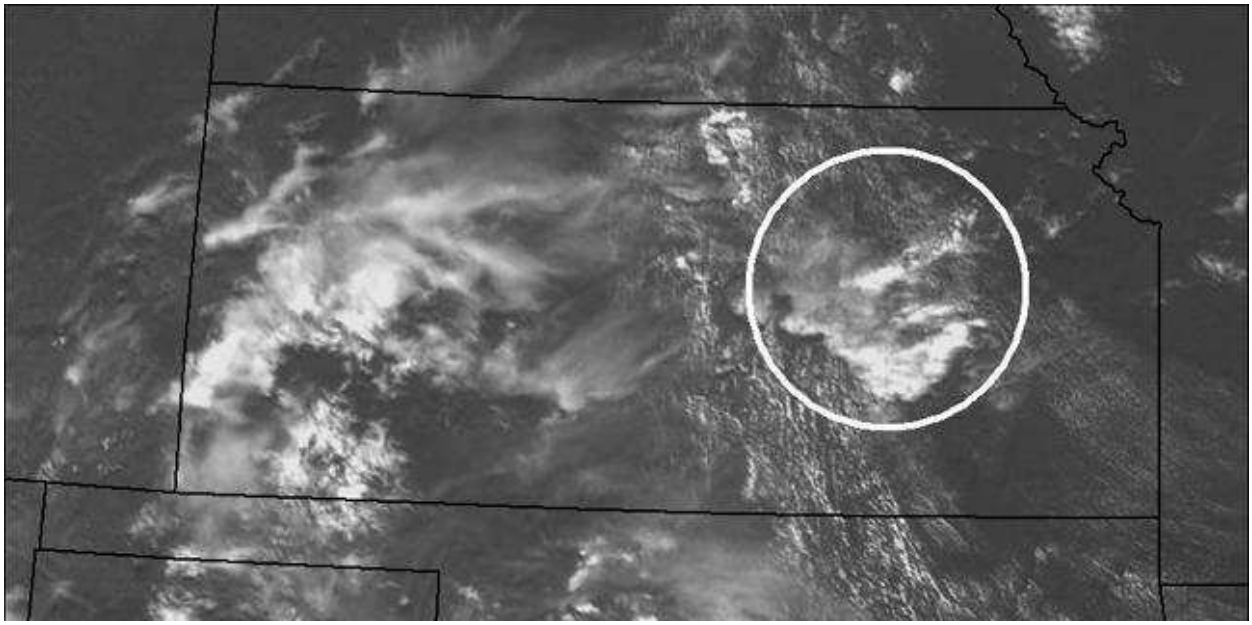

Figure 1: A Geostationary Operational Environmental Satellites-10 (GOES-10) image from 1631 UTC on 25 June 1996. The altocumulus cloud system, located in eastern Kansas, is circled. The aircraft entered the cloud system at 1634 UTC.

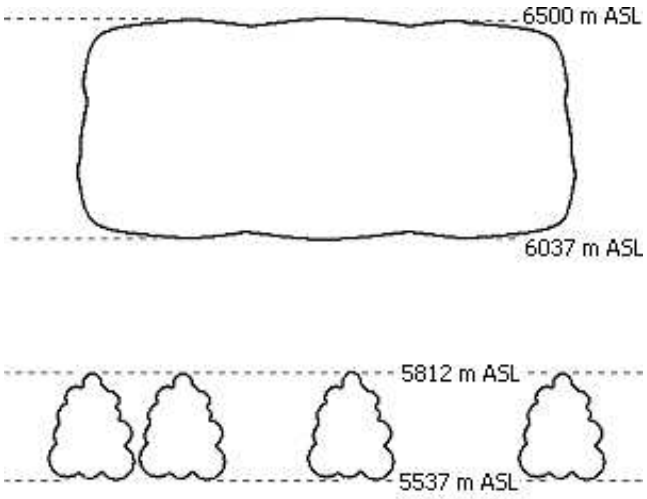


Figure 2: A drawing of the 25 June 1996 altocumulus cloud system. In most areas, there was a clear separation of several hundred meters between the lower and upper cloud layers.

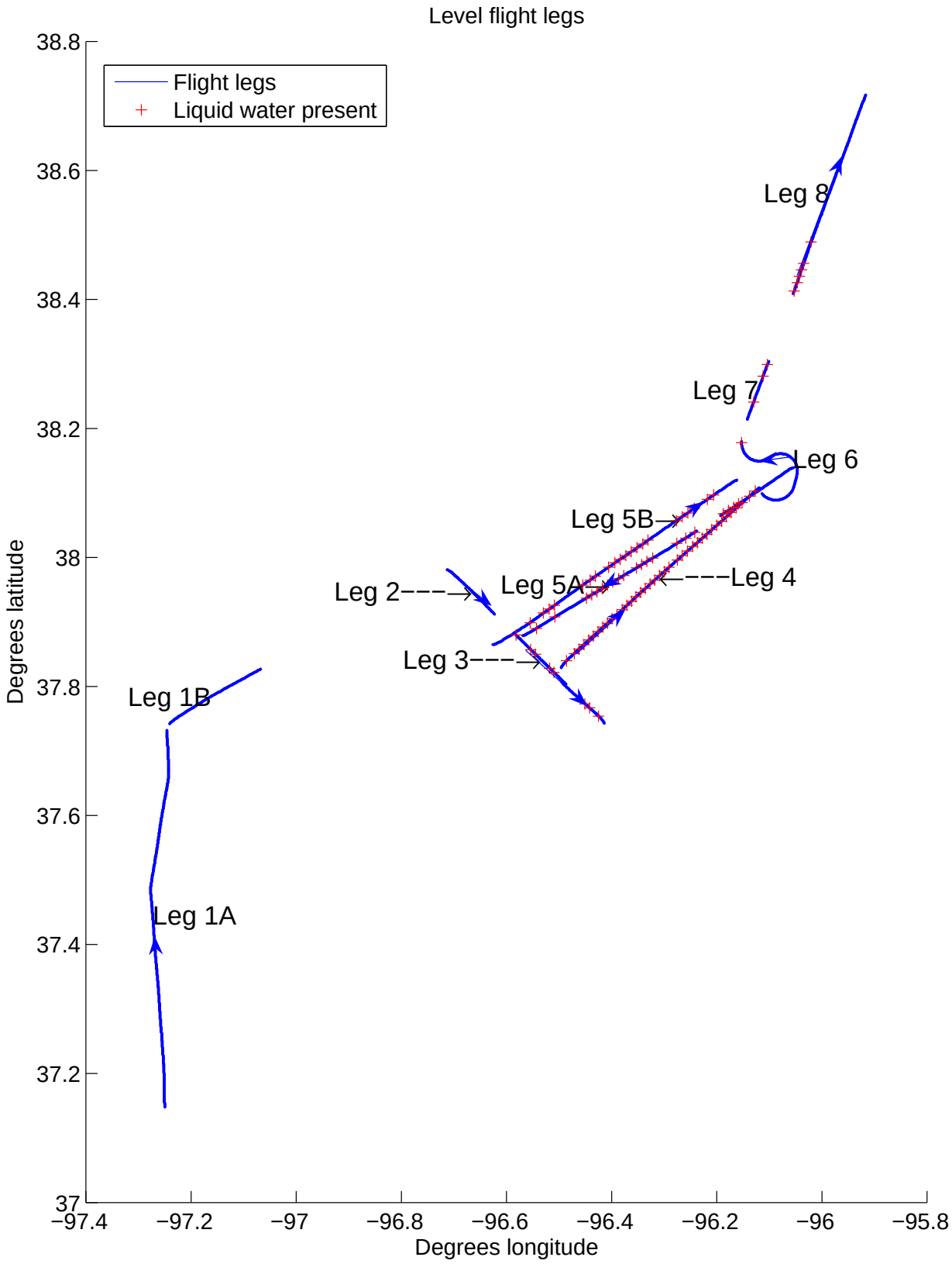


Figure 3: The path taken by the aircraft within the 25 June 1996 altocumulus cloud system. Each "leg" shown was level within 10 m and was at a constant heading within 20°. Crosses mark the locations where liquid water was sampled by the instruments aboard the aircraft.

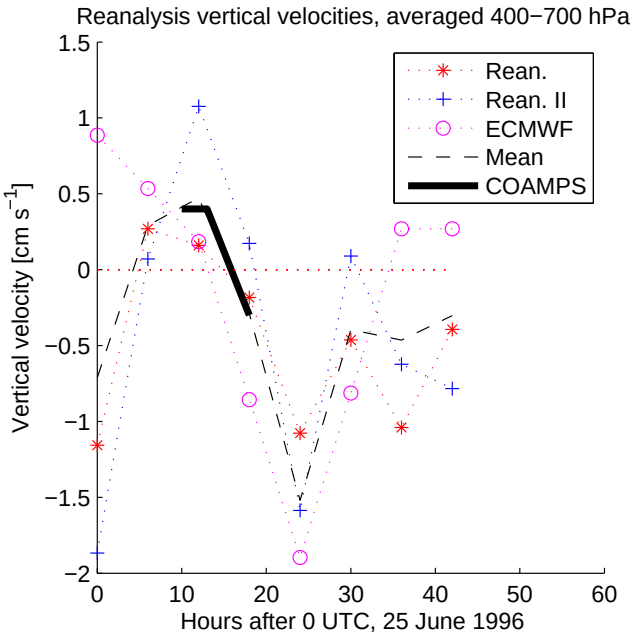


Figure 4: Large-scale vertical motion calculated at the location of the altocumulus cloud system on 25 and 26 June 1996 as interpolated from the NCEP Reanalysis (asterisks), NCEP Reanalysis-II (pluses), and ECMWF models (circles). The vertical motion used by COAMPS-LES (solid line) was an idealization of the mean of the reanalyses (thin dashed line).

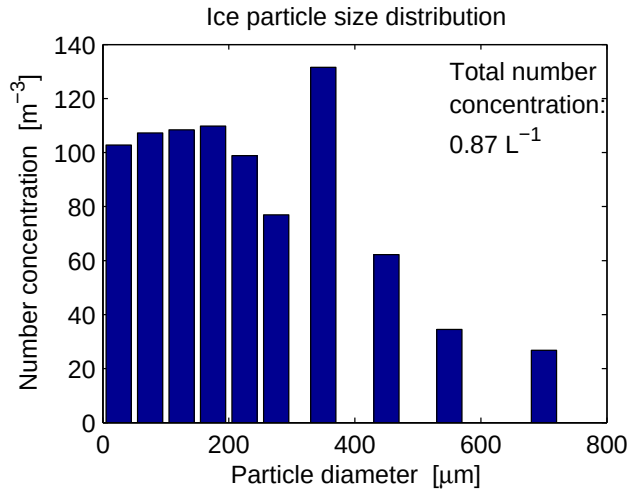


Figure 5: The number concentration of ice particles in twelve different bins in the stratiform layer, as measured by 2D-C and 2D-P probes. Smaller crystals were more prevalent than larger crystals, and the overall concentration of crystals of all sizes was measured to be 0.87 L$^{-1}$.

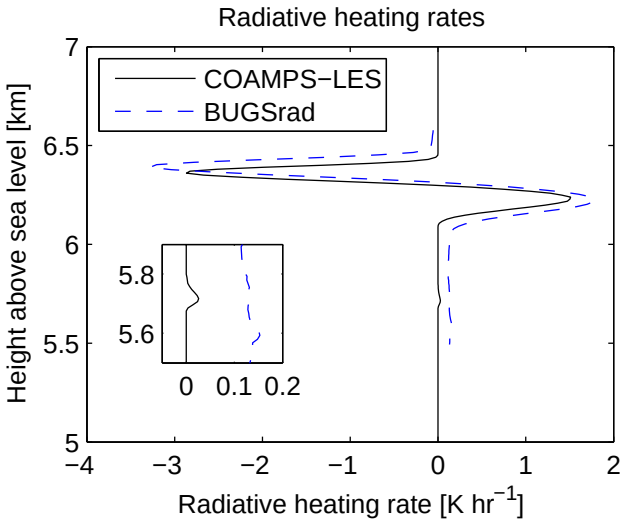


Figure 6: Radiative heating rates calculated by the COAMPS-LES analytic code and by BUGSrad, an independent radiative transfer code. Although the match is not exact, the qualitative agreement between the two codes is good.

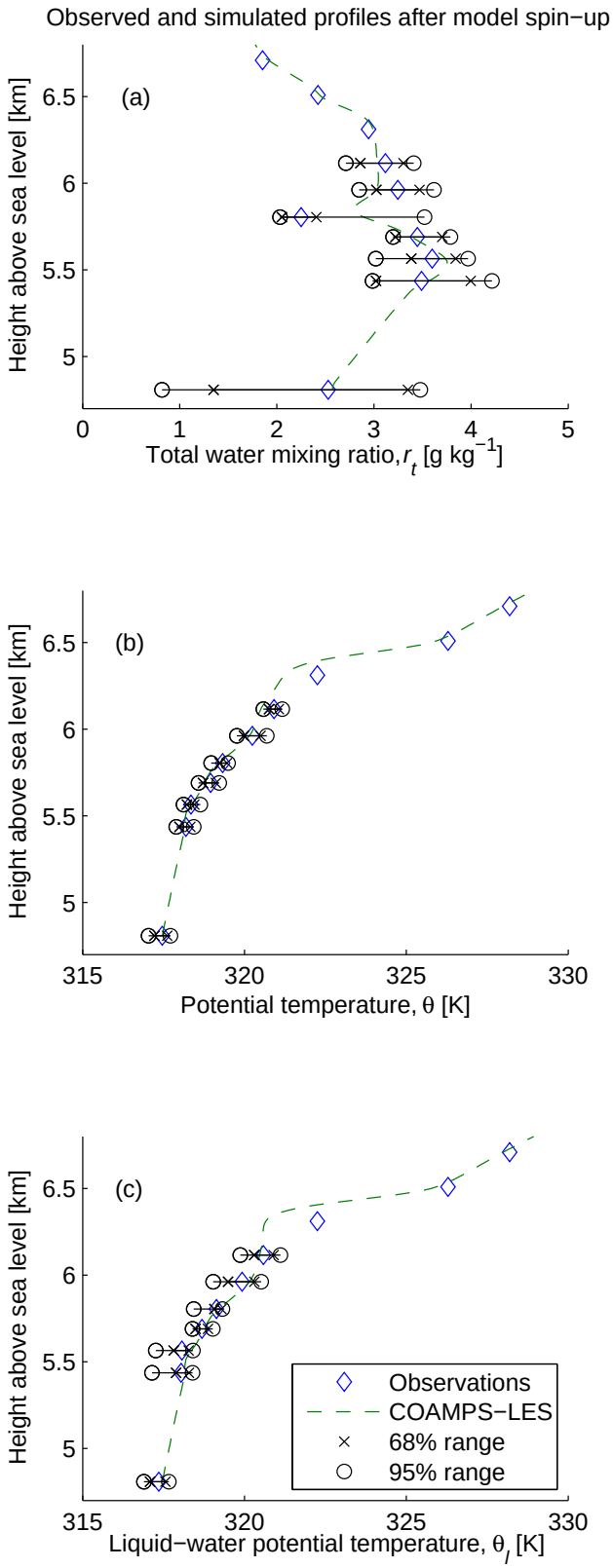


Figure 7: The (a) total water mixing ratio $r_t$, (b) potential temperature $\theta$, and (c) liquid-water potential temperature $\theta_l$ measured by the aircraft and computed by COAMPS-LES. The COAMPS-LES profiles are one-hour averages obtained immediately following model spin-up after the turbulence had equilibrated. Overall the model fields match the observations well, although the profile is "smoothed" by the turbulent mixing.

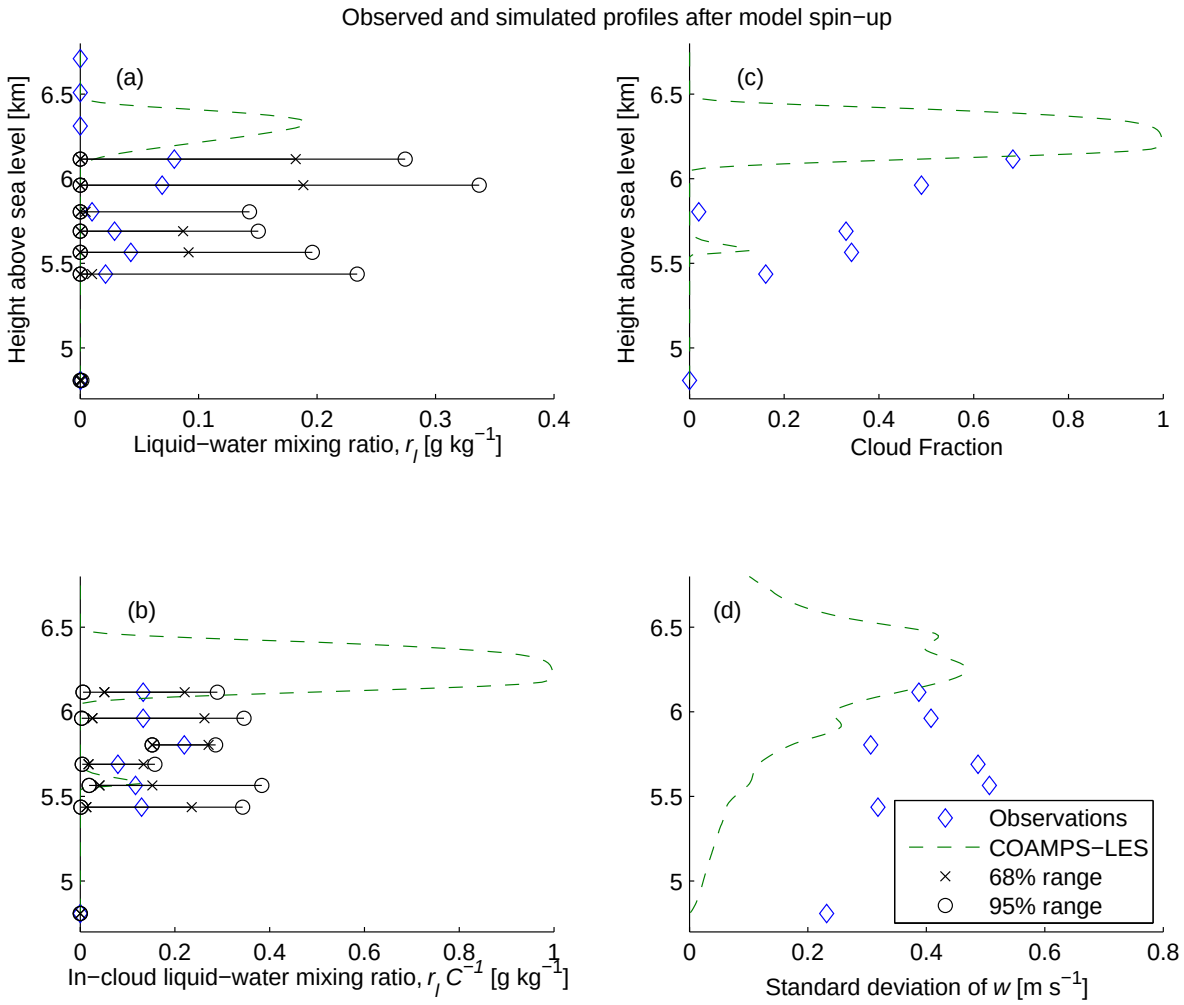


Figure 8: The (a) liquid-water mixing ratio $r_l$, (b) in-cloud liquid-water mixing ratio $r_l/C$, (c) cloud fraction, and (d) standard deviation of vertical velocity. The COAMPS-LES profiles are one-hour averages obtained immediately following spin-up, as in Figure 7. There is little turbulence in the model at low levels, which leads to a nearly homogeneous atmosphere. Since there are fewer pockets of very moist or very dry air, the $r_l$ is much lower in the model than in the observations. A better $r_l$ match in the cumuliform layer is given by the in-cloud liquid-water mixing ratio.

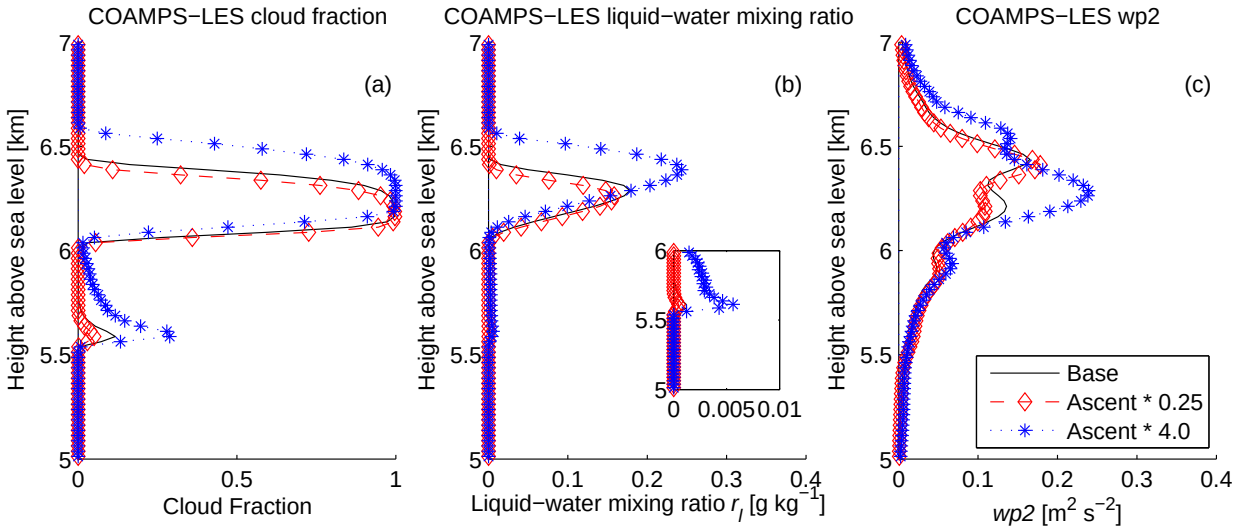


Figure 9: Dependence of (a) cloud fraction, (b) liquid-water mixing ratio, and (c) wp2 (i.e. $\overline{w'^2}$), averaged over the first hour following spinup, on ascent. Stronger ascent leads to higher cloud fractions, higher liquid water amounts, and stronger turbulence in the lower layer and a higher cloud base and cloud top in the upper layer.

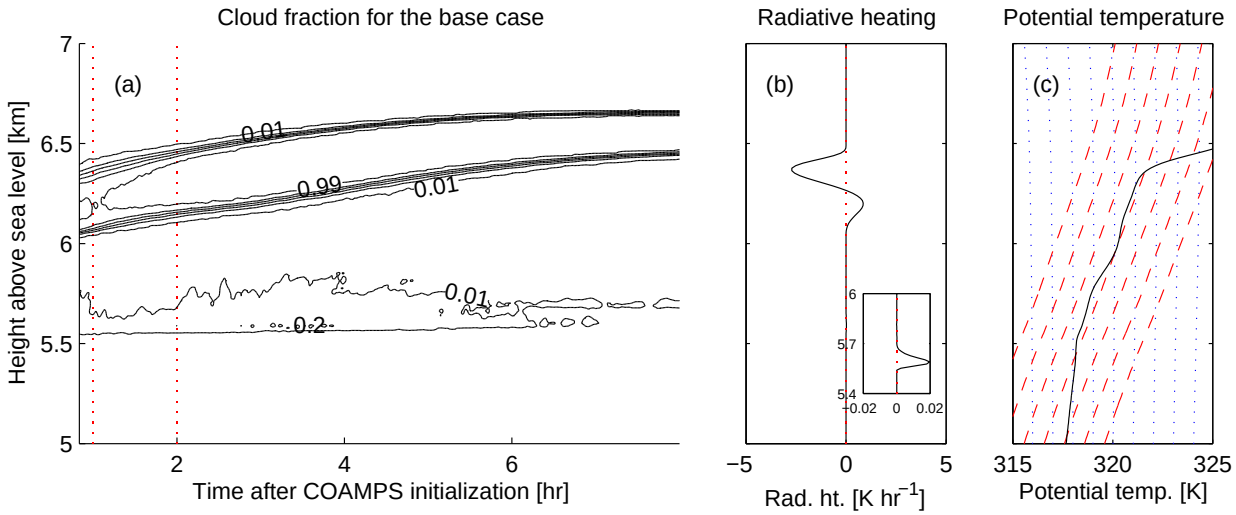


Figure 10: (a) The cloud fraction (time series), (b) radiative heating, and (c) potential temperature for the base case. The vertical dotted lines in the cloud fraction plot show the time interval over which the radiative heating and potential temperature plots are averaged. The vertical dotted line in the radiative heating plot shows the zero line. The vertical dotted lines in the potential temperature plot show lines of potential temperature for unsaturated parcels, and the diagonal dashed lines show lines of potential temperature for saturated parcels. The atmosphere is conditionally unstable in the lower layer and the gap between clouds but absolutely stable in the upper layer. The radiative heating profile predictably shows cooling at the upper cloud's top and warming at the upper cloud's base and very slight heating in the lower cloud.

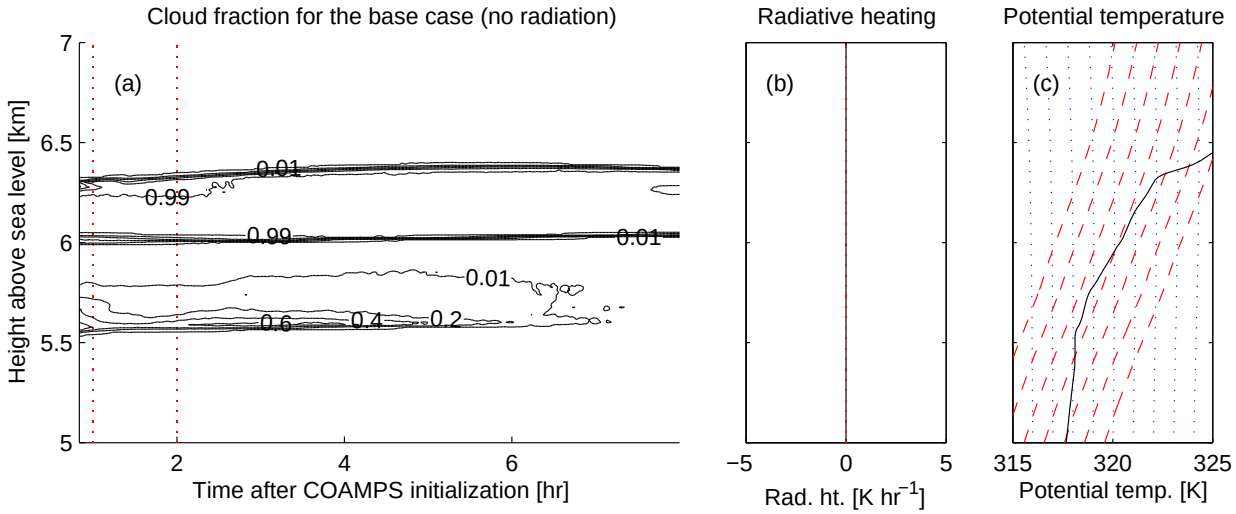


Figure 11: (a) The cloud fraction, (b) radiative heating, and (c) potential temperature for the base case with no radiation. With no radiative heating, much less turbulence is created. The base case sounding is conditionally unstable, so partial cloudiness still occurs. The cloud layers do not develop vertically but instead stay mostly stationary. When ascent is present, the cloud fraction reaches 0.6 near the bottom of the lower cloud, but when descent was present the cloud is killed quickly.

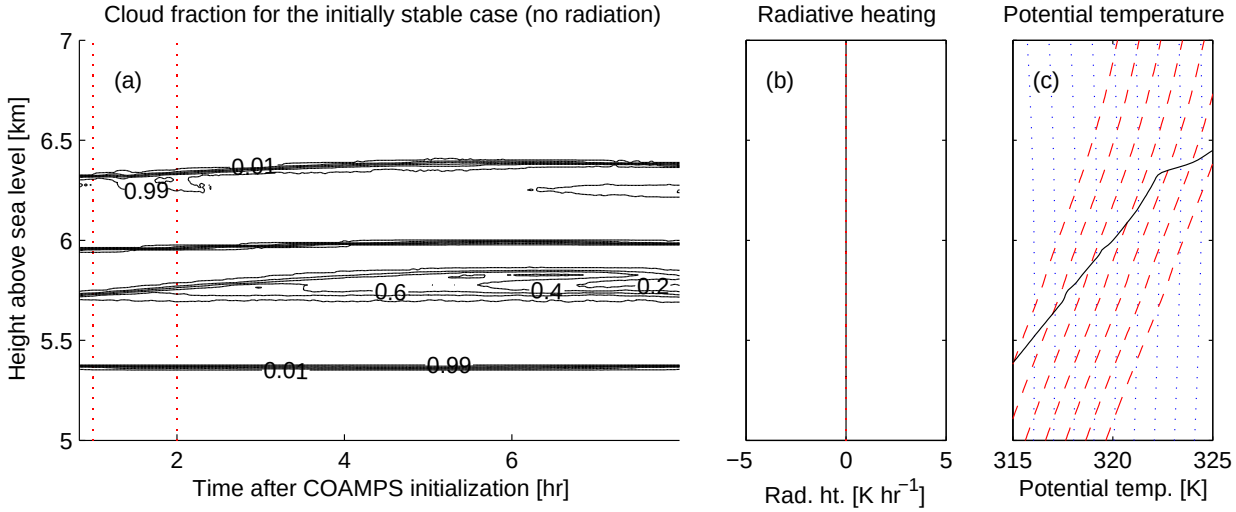


Figure 12: (a) The cloud fraction, (b) radiative heating, and (c) potential temperature for the initially stable case with no radiation. Since the layer is stable, it stays completely overcast for several hours. The top of the lower cloud layer becomes slightly unstable in time due to ascent, mixing, and evaporative cooling at cloud top and so its cloud fraction decreases slightly, but all of the portions of cloud which remain stable also remain at 100% cloud fraction.

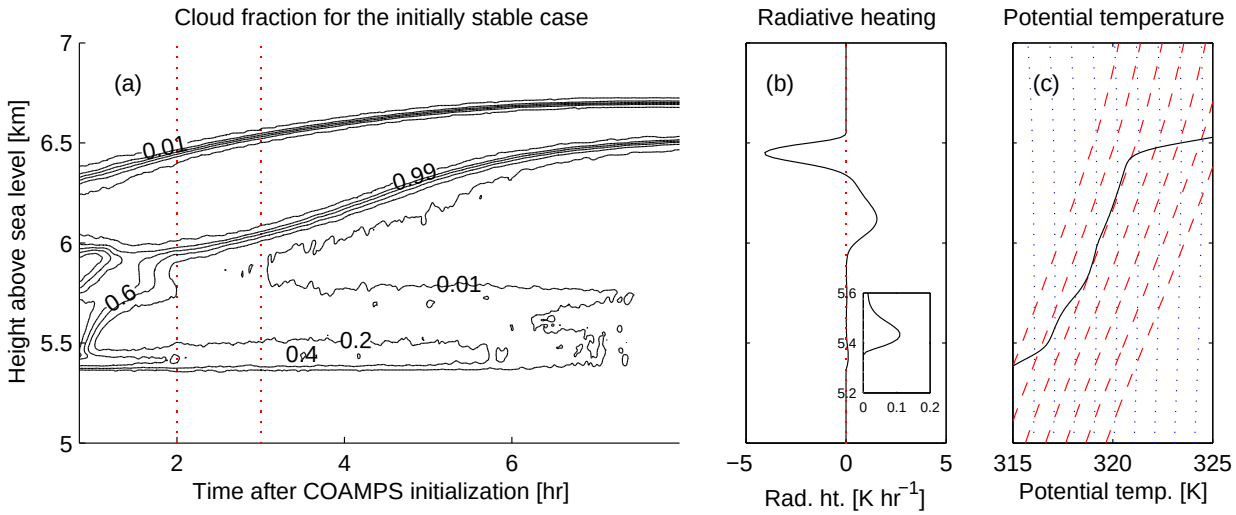


Figure 13: (a) The cloud fraction, (b) radiative heating, and (c) potential temperature for the initially stable case. The atmosphere becomes conditionally unstable in the lower layer but remains stable in the upper layer. The radiative heating profile shows warming within the lower cloud layer; this in-cloud heating causes instability to form, in turn creating partial cloudiness, even though the profile is stable and the cloud layer is at 100% cloud fraction at the initial time.

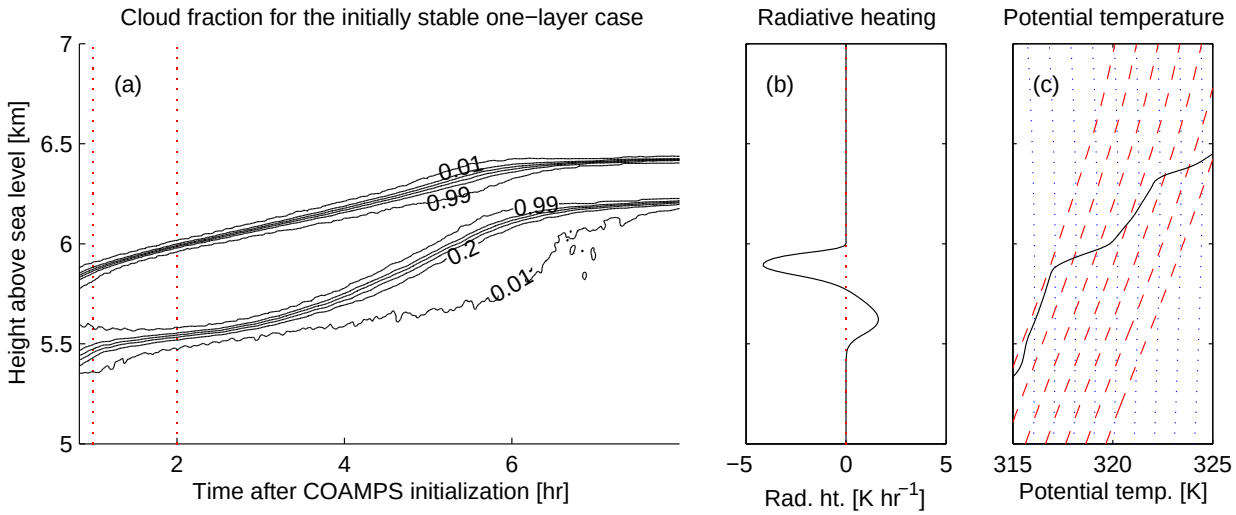


Figure 14: (a) The cloud fraction, (b) radiative heating, and (c) potential temperature for the initially stable one-layer case. There is radiative heating at and above cloud base but radiative cooling at and below cloud top, creating turbulence within cloud. Above cloud, however, the stable inversion is strengthened by the cloud-top cooling, preventing cloudy parcels from penetrating into and mixing with the dry air above cloud. Due to the lack of instability at cloud top and the associated lack of mixing between moist and dry air, the cloud remains at 100% cloud fraction.